



# Effect of organic acids precursors on the morphology and size of ZrO<sub>2</sub> nanoparticles for photocatalytic degradation of Orange G dye from aqueous solutions



Islam M. Ibrahim <sup>\*</sup>, Moustafa E. Moustafa, Mohamed R. Abdelhamid

Chemistry Department, Faculty of Science, Benha University, 13518, Egypt

## ARTICLE INFO

### Article history:

Received 24 July 2016

Received in revised form 25 August 2016

Accepted 31 August 2016

Available online 1 September 2016

### Keywords:

Zirconium oxide nanoparticles

XRD

HR-TEM

Photocatalytic degradation

Orange G dye

## ABSTRACT

Zirconium oxide nanoparticles were prepared by precipitation from different organic acid precursors (oxalic, tartaric, citric, succinic, malic, maleic and malonic) and ignition at 750 °C. The as-prepared samples were characterized by XRD, FT-IR, UV-Vis and HR-TEM techniques. XRD proved the crystalline monoclinic structure of the samples with average crystal sizes ranged from 7.1 nm (for citrate) to 35.1 nm (for maleic) precursor. The FT-IR spectra of the nanooxides showed the characteristic bands due to  $\nu_{\text{OH}}$ ,  $\delta_{\text{OH}}$  and  $\nu_{\text{Zr-O}}$  at 3444, 1633 and 498  $\text{cm}^{-1}$ , respectively. The UV-Vis spectra proved the semiconductor nature of the samples with optical energy gap ranging from 1.80 to 4.30 eV. One of the prepared samples was tested as catalyst for the photodegradation of Orange G dye in wastewater samples in presence of H<sub>2</sub>O<sub>2</sub> where 100% removal of the dye was obtained after about 180 min.

© 2016 Elsevier B.V. All rights reserved.

## 1. Introduction

In recent years zirconium oxides play an important role in applied chemistry due to their vast applications such as semiconductors [1], alkylation of aromatic compounds [2], oxidation of dimethyl sulfide [3], biodiesel applications [4], biological applications [5], glaze applications [6], purification of oils [7] and photocatalytic degradation of organic pollutants such as dyes and 2,4-dichlorophenol [8,9]. Almost every industrial dye process involves a solution of a dye in water, in which the fabrics are dipped or washed. After dyeing a batch of fabric, it's cheaper to dump the used water – dye effluent – than to clean and reuse the water in the factory. So dye factories across the world are dumping millions of tons of dye effluent into rivers. Dyes are so problematic because the families of chemical compounds that make good dyes are also toxic to humans or are considered deadly poisons [10]. Photocatalytic degradation of dyes from aqueous solution is considered one of the most effective methods for water treatment especially using nanosized metal oxides as catalysts [11,12]. Among of these oxides zirconium oxide possess high catalytic activity toward organic pollutants due to its high surface area, crystallinity, different morphologies and easily separation of electron hole pairs which are necessary for generating free radicals which decompose the organic pollutants [13,14]. There are various methods for preparing zirconium oxides such as sol gel, hydrothermal, flame spray and chemical vapor deposition [15–18]. Using

inexpensive organic acids in preparing nanooxides via precipitation – ignition method is considered excellent effective economic procedure and produce nanosized oxides characterized by their small crystal size and different morphologies [19]. To the best of our knowledge there are no papers in studying the effect of different inexpensive organic acids in the preparation of nanosized zirconium oxide. In this paper we study the effect of different inexpensive organic acids (oxalic, tartaric, citric, succinic, malic, maleic and malonic) on both of crystal size and morphology of nanosized zirconium oxides and one of the synthesized oxides was tested as a catalyst for photocatalytic degradation of Orange G dye from aqueous solutions.

## 2. Experimental

### 2.1. Chemicals

All chemicals used in the present study were of the highest quality (Merck, Aldrich or Fluka) and were used without further purification. Freshly bidistilled water was used whenever water is necessary.

### 2.2. Synthesis of zirconium oxide nanoparticles

Zirconium oxide nanoparticles (Z1–Z7) were prepared via the precipitation of 50 ml of 0.1 M zirconyloxochloride using drop by drop addition of 50 ml of 0.2 M of different organic acids viz. oxalic (Z1), tartaric (Z2), citric (Z3), succinic (Z4), malic (Z5), maleic (Z6) and malonic (Z7) respectively, in 1: 2 M ratio. The mixtures were stirred for 1 h. and the

<sup>\*</sup> Corresponding author.

E-mail address: [islam.mustafa@fsc.bu.edu.eg](mailto:islam.mustafa@fsc.bu.edu.eg) (I.M. Ibrahim).

**Table 1**  
Elemental analysis and FT-IR of samples Z1–Z7 prepared using oxalic, tartaric, citric, succinic, malic, maleic and malonic acids, respectively before ignition.

Sample	Precipitant	Precipitated form (M wt)	Elemental analysis		FT-IR ( $\text{cm}^{-1}$ )				
			C% Calc (found)	H% Calc (found)	$\nu_{\text{OH}}$	$\nu_{\text{C=O}}$	$\nu_{\text{Zr-O}}$	$\nu_{\text{C=C}}$	$\delta_{\text{CH}}$
Z1	Oxalic	$[\text{ZrC}_4\text{O}_8] \cdot \text{H}_2\text{O}$ (285)	17.9 (18.2)	0.70 (0.86)	3221.25	1628.26	547.54 436.10	–	–
Z2	Tartaric	$[\text{ZrC}_8\text{H}_8\text{O}_{12}] \cdot \text{H}_2\text{O}$ (405)	24.80 (25.5)	2.06 (2.34)	3410.42	1739.94	551.60 481.41	–	1137.80- 684.04
Z3	Citric	$[\text{ZrC}_{12}\text{H}_{12}\text{O}_{14}] \cdot \text{H}_2\text{O}$ (489)	30.57 (31.12)	2.54 (2.82)	3408.48	1670.30	606.10 474.92	–	1276.55- 810.78
Z4	Succinic	$[\text{ZrC}_8\text{H}_8\text{O}_8] \cdot \text{H}_2\text{O}$ (341)	29.72 (30.34)	2.47 (2.59)	3207.62	1693.80	544.82 480.87	–	1201.64- 637.45
Z5	Malic	$[\text{ZrC}_8\text{H}_6\text{O}_{10}] \cdot \text{H}_2\text{O}$ (373)	27.04 (27.34)	1.69 (1.82)	3415.85	1629.12	577.13 475.18	–	1202.36- 663.90
Z6	Maleic	$[\text{ZrC}_8\text{H}_4\text{O}_8] \cdot \text{H}_2\text{O}$ (337)	30.01 (30.21)	1.25 (1.37)	3377.84	1674.26	579.85 490.67	1577.96	1213.37- 648.58
Z7	Malonic	$[\text{ZrC}_6\text{H}_4\text{O}_8] \cdot \text{H}_2\text{O}$ (313)	24.41 (24.81)	1.36 (1.42)	3396.92	1559.31	650.00 463.99	–	1171.72- 955.07

precipitates formed were filtered, washed thoroughly using bidistilled water, air dried then ignited at 750 °C for 5 h to produce the corresponding zirconium oxide nanoparticles.

### 2.3. Physical measurements

FT-IR spectra of both of the precipitated and ignited samples were recorded on a Nicolet iSio FT-IR spectrophotometer in the 4000–400  $\text{cm}^{-1}$  region using KBr disk technique (Chemistry department, Faculty of science, Benha University, Egypt). Electronic absorption spectra of the prepared nanooxides were recorded on a Jasco (V-530) UV-Vis spectrophotometer (Chemistry department, Faculty of Science, Benha University, Egypt). Thermogravimetric analyses (TG) for the organic precursors were recorded on Shimadzu TA-60 WS thermal analysis (Micro analytical unit, Menofia University, Egypt). Elemental analysis for C and H of the nanooxides were carried out using Elementer

Vario EL III Carlo Erba 1108 instrument (The Regional Center for Mycology and Biotechnology, Al-Azhar University, Cairo, Egypt). X-ray powder diffraction (XRD) were recorded on a 18 kW diffractometer (Bruker; model D8 Advance) with monochromated Cu  $K_{\alpha}$  radiation ( $\lambda$ ) 1.54178 Å (Central metallurgical research institute, Helwan, Egypt). The HR-TEM images of the prepared zirconium oxides were taken on a transmission electron microscope (JEOL; model 1200 EX) at an accelerator voltage of 220 kV (Egyptian Petroleum Research Institute, Cairo, Egypt).

### 2.4. Photocatalytic activity measurements

The photocatalytic degradation of 20 ppm Orange G dye aqueous solution was performed using the smallest crystal sized zirconium oxide (Z3) sample (prepared from citric acid). For a typical photocatalytic experiment, 100 mg of Z3 photocatalyst was added to 25 ml of 20 ppm

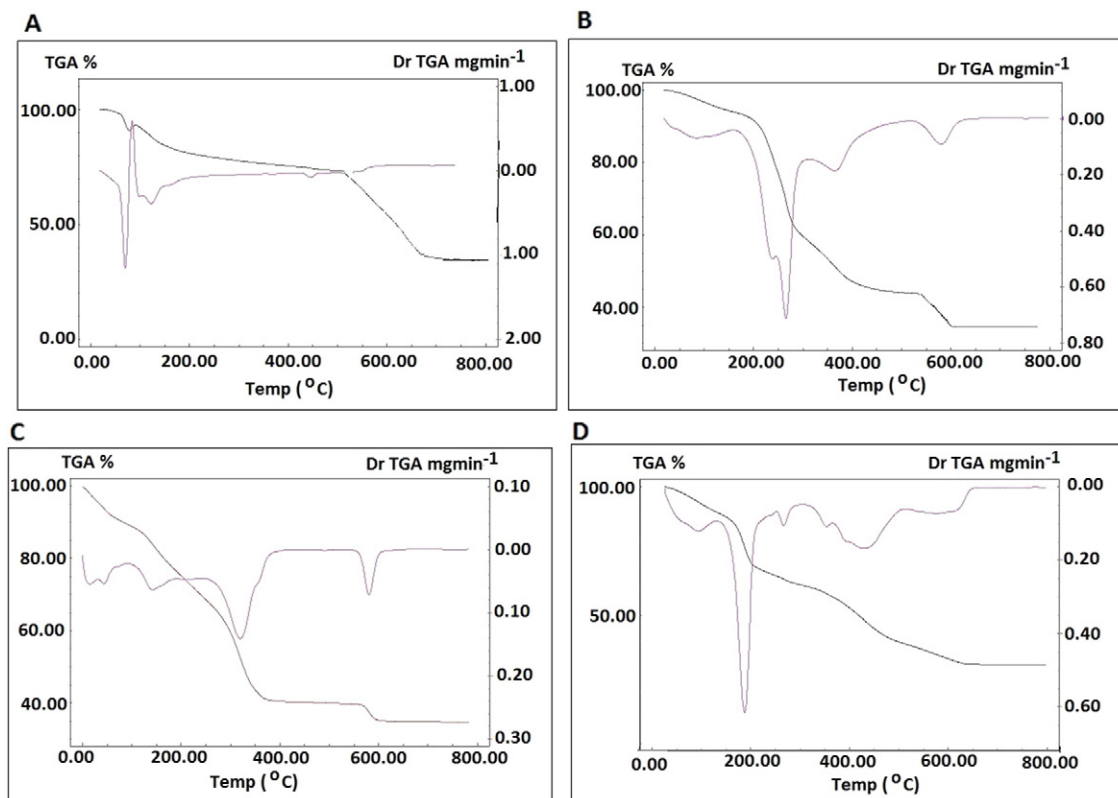


**Fig. 1.** Thermal analysis of samples Z1–Z4 prepared using (A) oxalic (B) tartaric (C) citric (D) succinic acids before ignition.

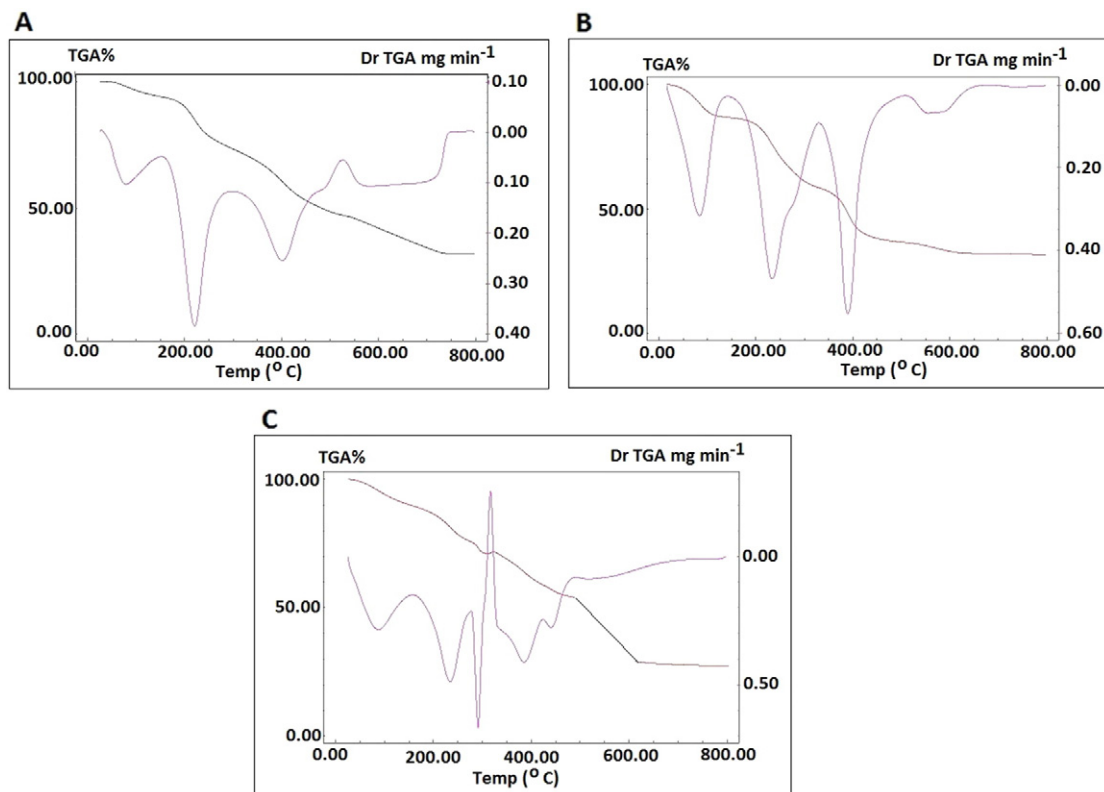
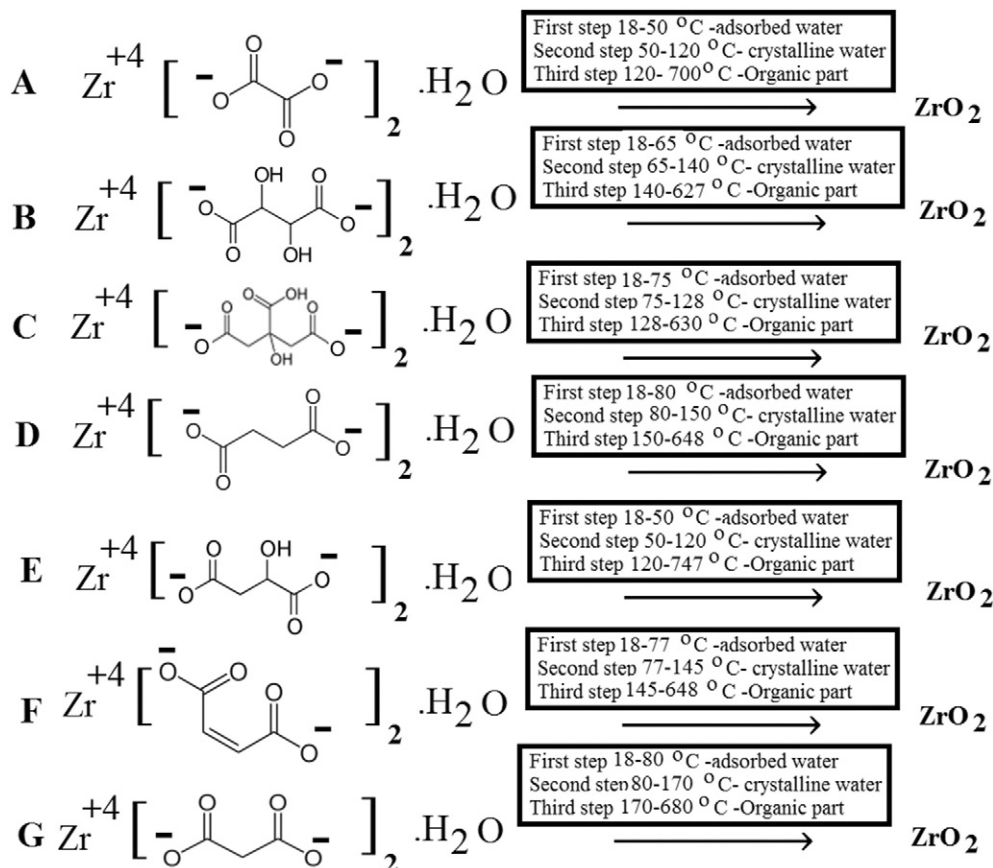


Fig. 2. Thermal analysis of samples Z5–Z7 prepared using (A) malic (B) maleic (C) malonic acids before ignition.



Scheme 1. Mechanism of formation of  $\text{ZrO}_2$  nanoparticles (Z1–Z7) using (A) oxalic (B) tartaric (C) citric (D) succinic (E) malic (F) maleic (G) malonic.

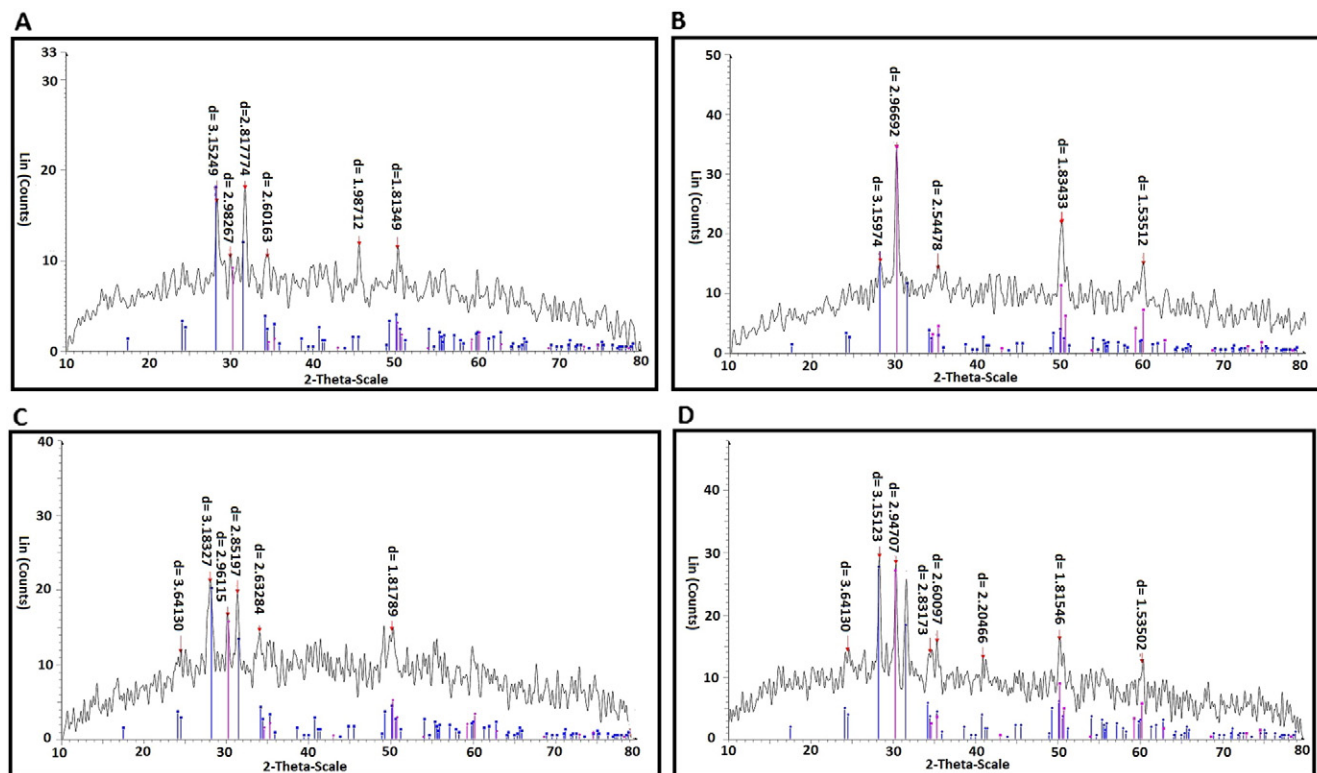


Fig. 3. XRD of samples Z1–Z4 prepared using (A) oxalic (B) tartaric (C) citric (D) succinic acids.

aqueous dye solution which was kept in dark for 6 h to allow the system to reach an adsorption desorption equilibrium then 2 ml of 0.5 M hydrogen peroxide solution was added. The degradation process was investigated in a Pyrex beaker under the UV illumination using a 250 W xenon

arc lamp (Thoshiba, SHLS-002) ( $\lambda = 365$  nm). After recovering the catalyst by centrifugation, the light absorption of the clear solution was measured at 485 nm ( $\lambda_{\max}$  for Orange G dye) at different time intervals using a UV-Vis spectrophotometer.

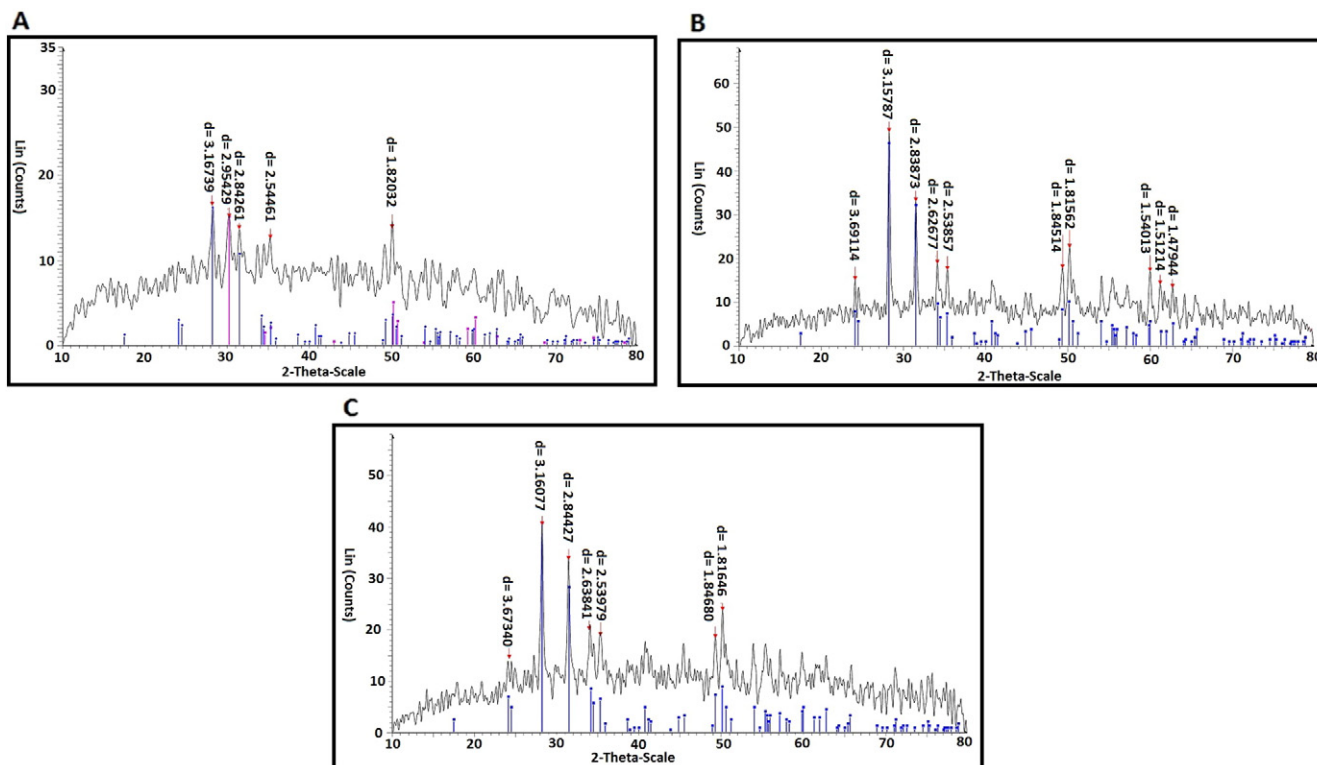


Fig. 4. XRD of samples Z5–Z7 prepared using (A) malic (B) maleic (C) malonic acids.

### 3. Results and discussion

#### 3.1. Elemental (C and H) and thermal (TGA) analysis

Results of the elemental analysis (C and H), Table 1, show satisfactory agreement with the proposed structure confirming the molecular weight of samples. Inspection of TG curves (Figs. 1 and 2) shows that the organic acid salt precursors of zirconium degrade thermally through three main steps; the first within the temperature range 50–100 °C due to the removal of physically adsorbed water molecules. The second step within the temperature range 120–150 °C is due to the removal of water of crystallization along with the evolution of CO<sub>2</sub> gases evolving from the organic precursors in the beginning of their thermal decomposition as a final step. The later led to the formation of zirconium oxides nanoparticles (Z1–Z7) at 700, 627, 630, 648, 747, 648 and 680 °C, for samples prepared from oxalic, tartaric, citric, succinic, malic, maleic and malonic acids, respectively (Scheme 1). So, all the samples were ignited at 750 °C to ensure complete degradation of organic moiety, to produce the corresponding zirconium nanooxides.

#### 3.2. X-ray diffraction (XRD) studies

The crystalline structures of zirconium oxides samples (Z1–Z7) were characterized using XRD as clarified in Figs. 3 and 4. The diffraction pattern of all samples includes not only the peak positions but also their relative intensities which can be perfectly indexed into the monoclinic type phase of zirconium oxide with cell constants:  $a = 5.1501 \text{ \AA}$ ,  $b = 5.2077 \text{ \AA}$  and  $c = 5.3171 \text{ \AA}$  (space group  $P2_1/c$ , JCPDS card 01-088-

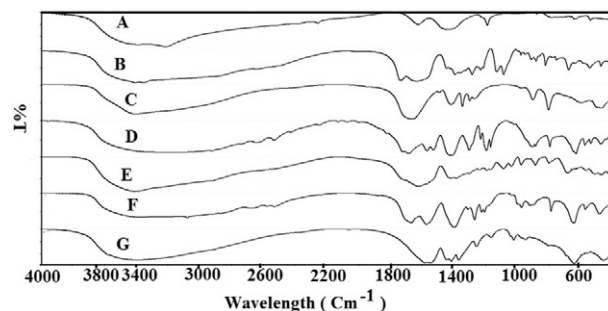


Fig. 6. FT-IR of samples Z1–Z7 prepared using (A) oxalic (B) tartaric (C) citric (D) succinic (E) malic (F) maleic (G) malonic acids before ignition.

2390). The obtained data are in agreement with those published earlier by Yashima et al. [20]. No characteristic peaks of other impurity phases were appeared, indicating that the prepared samples are of high purity. The average crystal size was estimated using the Debye–Scherrer formula [21]:

$$D = 0.9\lambda / \beta \cos\theta_B$$

where  $\lambda$ ,  $\beta$ ,  $\theta_B$  are the X-ray wavelength, the full width at half maximum (FWHM) of the diffraction peak and the Bragg diffraction angle, respectively. From the X-ray diffraction data, the estimated average crystal size of zirconium oxide nanoparticles (Z1–Z7), prepared using different organic acids; oxalic, tartaric, citric, succinic, malic, maleic and malonic

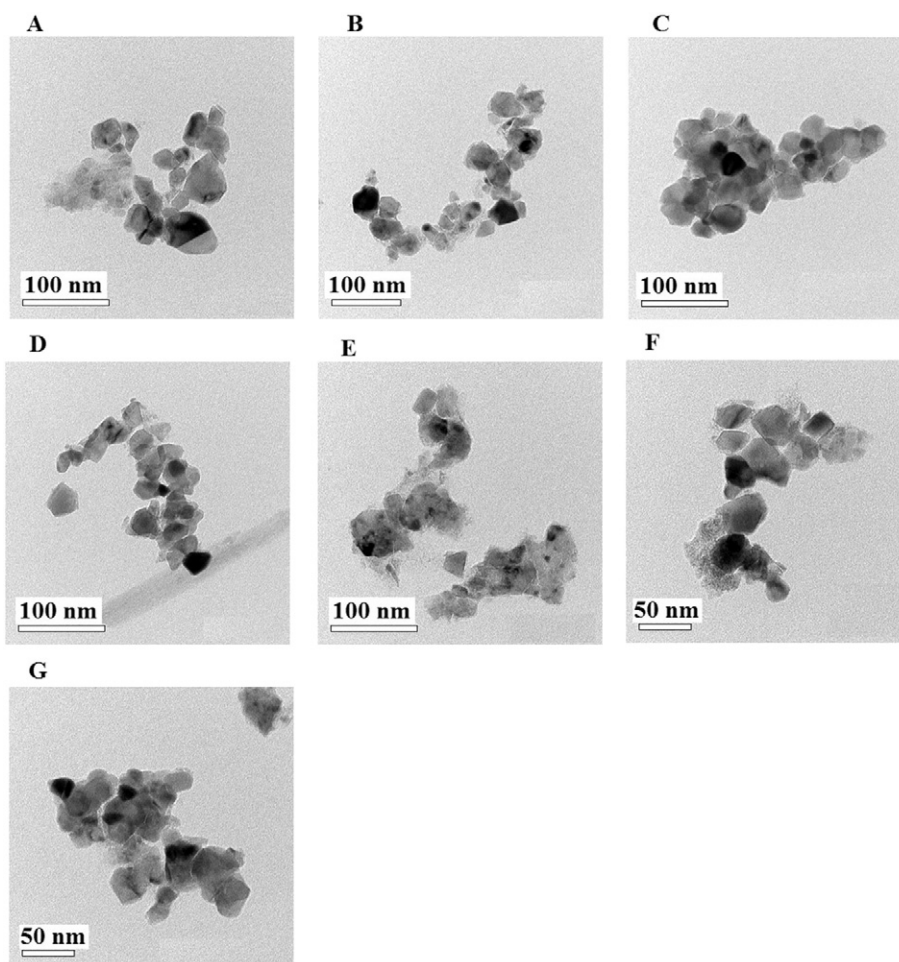


Fig. 5. HR-TEM of samples Z1–Z7 prepared using (A) oxalic (B) tartaric (C) citric (D) succinic (E) malic (F) maleic (G) malonic acids.

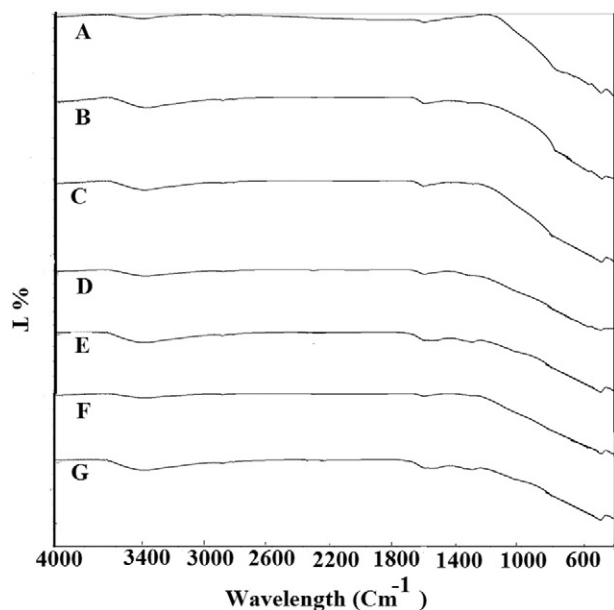


Fig. 7. FT-IR of samples Z1–Z7 prepared using (A) oxalic (B) tartaric (C) citric (D) succinic (E) malic (F) maleic (G) malonic acids.

as precipitants were found to be 9.9, 8.3, 7.1, 11.3, 7.3, 35.6 and 26.0 nm, respectively. So; the average crystal size increases in the order Z3 (Citric) < Z5 (Malic) < Z2 (Tartaric) < Z1 (Oxalic) < Z4 (Succinic) < Z7 (Malonic) < Z6 (Maleic) indicating the importance of organic acids in controlling the crystal size of nanooxides.

### 3.3. HR-TEM studies

The morphologies and microstructures of the as-prepared samples were investigated with HR-TEM (*cf.* Fig. 5). The images reveal that the products consist of cubical particles with some irregular shapes of average sizes of 9.5 and 37.6 nm for Z1 and Z6, spherical particles with the average size 8.7 and 7.7 nm for the nanoparticle Z2 and Z3 and spherical-cubical particles with the average size 13.3, 7.5 and 28 nm for Z4, Z5 and Z7, respectively. All images are appeared to be of high crystallinity. The previously discussed data showed that the choice of organic precipitants has an effective role on both crystal size and morphology of the prepared nanooxides.

### 3.4. FT-IR studies

The Fourier transform infrared (FT-IR) spectra of the oxide nanoparticles were scanned and compared to those of the organic precursors before ignition, (*cf.* Figs. 6 and 7). The spectra of the latter showed the vibrational frequencies of the functional groups ( $\nu_{\text{OH}}$ ,  $\nu_{\text{C=O}}$ ,  $\nu_{\text{Zr-O}}$ ,  $\nu_{\text{C=C}}$  and  $\delta_{\text{CH}}$ ) as shown in Table 1 which disappeared after ignition. In the spectra of the nanooxides, the broad band within the range 3436–3456  $\text{cm}^{-1}$  is due the stretching vibration of the O–H group of physically adsorbed water molecule on the surface. The strong absorption bands near 1633  $\text{cm}^{-1}$  are assigned to H–O–H bending vibrations mode. The IR spectra of transition metal oxides are expected to exhibit the characteristic absorption bands in the shortwave region around 500  $\text{cm}^{-1}$  due to M–O stretching frequencies. The IR bands within the range 529–498  $\text{cm}^{-1}$  for all samples could be attributed to the stretching vibration of the Zr–O of zirconium atoms in the tetragonal environment of the O atom [22].

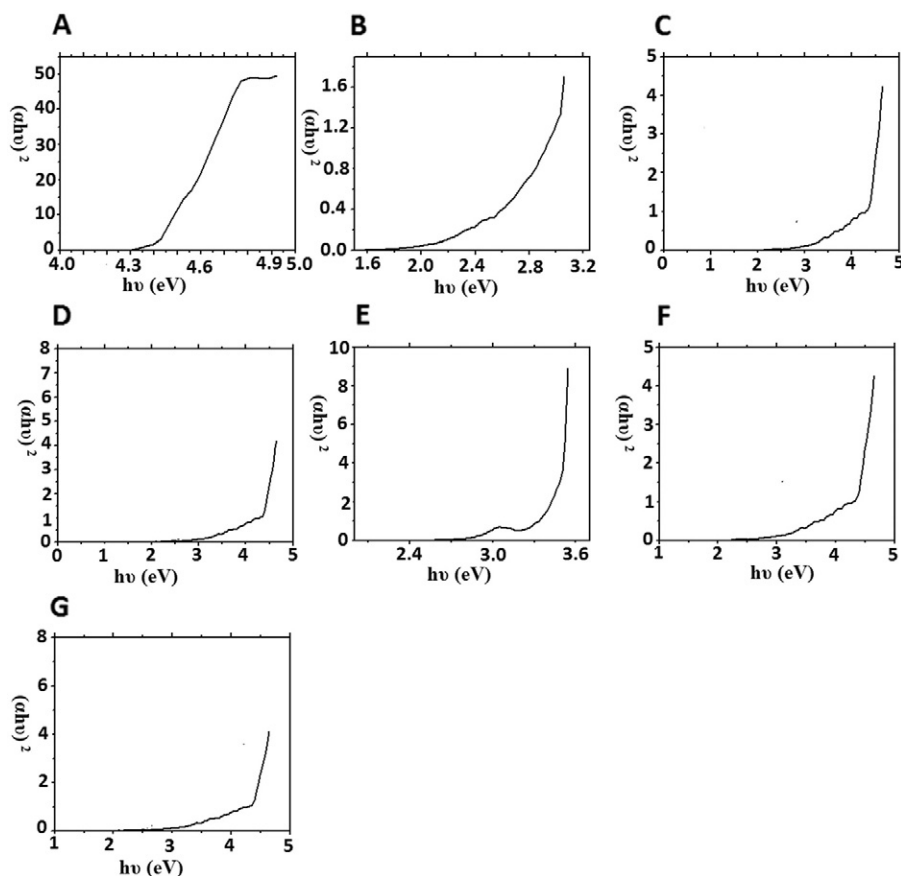


Fig. 8. Optical energy gap of samples Z1–Z7 prepared using (A) oxalic (B) tartaric (C) citric (D) succinic (E) malic (F) maleic (G) malonic acids.

### 3.5. Optical properties of zirconium oxide nanoparticles

UV–Vis absorption spectra of the prepared zirconium oxides were carried out in nujoll mull in order to determine their optical energy gap. The optical energy gaps ( $E_g$ ) can be calculated using the following equation:

$$(\alpha h\nu)^n = K (h\nu - E_g)$$

where  $\alpha$  is the absorption coefficient,  $K$  is a constant,  $E_g$  is the band gap and  $n$  is an integer equals either 2 for a direct allowed transition or 1/2 for an indirect allowed transition. For the prepared zirconium oxide nanoparticles, direct allowed transitions are the predominant and hence  $(\alpha h\nu)^2$  are plotted versus  $h\nu$ , as shown in Fig. 8. The extrapolation of each graph to  $(\alpha h\nu)^2 = 0$  gives the direct optical energy gaps ( $E_g$ ) which were found to be 4.30, 1.80, 2.70, 3.00, 2.70, 2.80 and 2.90 eV for the nanooxides Z1 to Z7, respectively. These values proved that the prepared zirconium oxides nanoparticles are semiconductors and are in an excellent agreement with the reported data [23].

### 3.6. Photocatalytic activity of zirconium oxide nanoparticles

The photodegradation efficiency of selected zirconium oxide nanoparticle (sample Z3; prepared from citric acid as organic precursor) was tested using Orange G (OG) as model. 25 ml solution containing the OG dye (20 ppm) and the nanoparticle oxide (100 mg) was photo irradiated by UV light at different conditions, namely; (UV + H<sub>2</sub>O<sub>2</sub> + Z3), (UV + H<sub>2</sub>O<sub>2</sub>), (UV only), (UV + Z3). At periodic intervals of time, aliquots of the sample were withdrawn and the

absorption spectra were recorded. Clearly, the absorbance decreases (c.f. Fig. 9; A, B, C and D, respectively) and the photodegradation efficiency increases (reaching a plateau) as a function of time. The results showed that the maximum percent of degradation of OG dye was 100% after 270 min in case of (UV + H<sub>2</sub>O<sub>2</sub>) (Fig. 9B), 19% after 210 min in case of UV only (Fig. 9C) and 23% after 180 min in case of (UV + Z3) (Fig. 9D) while, almost 100.00% of the dye was decomposed under UV illumination in the presence of hydrogen peroxide and Z3 catalyst within 180 min (as shown in Fig.9E) indicating the very high efficiency of Z3 compared with others cited in literature [24].

The mechanism of photodegradation process in the presence of UV only, (Z3 + UV) and (UV + Z3 + H<sub>2</sub>O<sub>2</sub>) has been showed in Scheme 2. After the dye absorbs UV–light only, the excited Orange G reduces O<sub>2</sub> to O<sub>2</sub><sup>-</sup>; which in turn reacts with a proton (from the autoprotolysis of the solvent water) to generate OOH<sup>•</sup>. In total, the cationic dye radical is degraded to CO<sub>2</sub>, H<sub>2</sub>O and mineral acids via intermediate. They also explained OOH<sup>•</sup> and OH<sup>•</sup>, which are important for the complete degradation of the orange G dye [24]. Photocatalytic degradation of Orange G dye in the presence of (Z3 + UV) usually includes the separation of electron hole pairs and the subsequent reduction–oxidation reactions under UV–light irradiation, electrons and holes are generated on the surface of zirconium oxide. The electrons scavenged by the adsorbed molecular oxygen species, and the holes trapped by water or adsorbed Orange G molecules. Then Orange G dye is degraded directly by the effect of photogenerated oxidants [24]. Adding hydrogen peroxide in the presence of Z3 and UV increases the photodegradation rate of Orange G dye because the direct decomposition of hydrogen peroxide under UV light generate OH<sup>•</sup>, which directly oxidize Orange G dye as shown in Scheme 2. It is noteworthy that the advantage of using nanosized

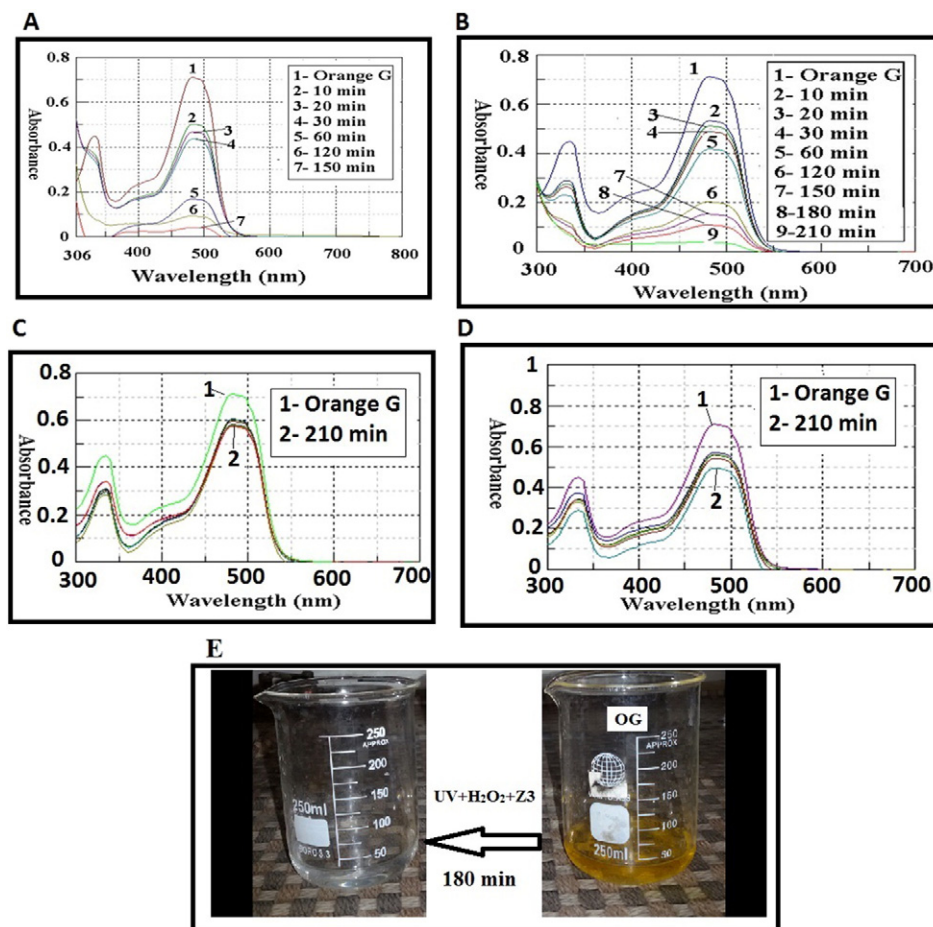
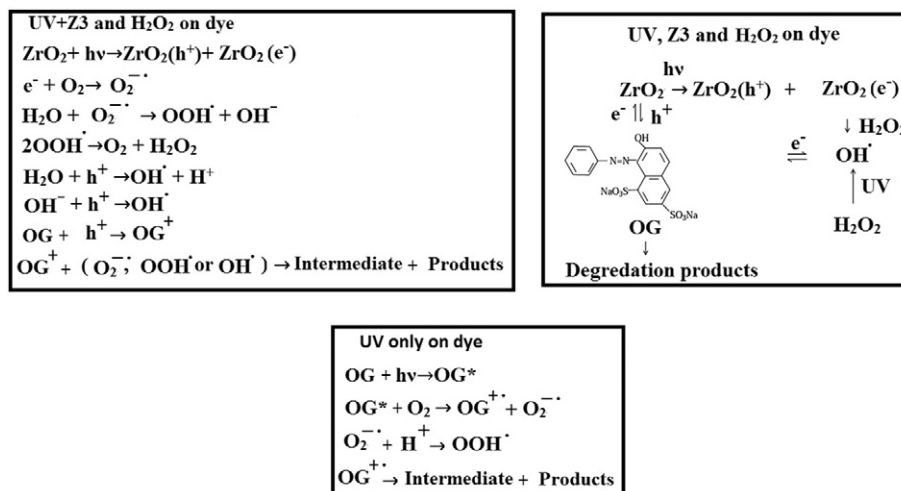


**Fig. 9.** Photocatalytic degradation of OG dye (A) using (UV + H<sub>2</sub>O<sub>2</sub> + Z3), (B) using (UV + H<sub>2</sub>O<sub>2</sub>), (C) using (UV only), (D) using (UV + Z3) (E) Complete de-colorization of OG dye after 180 min using (UV + H<sub>2</sub>O<sub>2</sub> + Z3). (For interpretation of the references to color in this figure legend, the reader is referred to the web version of this article.)



**Scheme 2.** Proposed reactions for the photodegradation of OG dye in the presence of UV only, (Z3 + UV) and (UV + Z3 + H<sub>2</sub>O<sub>2</sub>).

zirconium oxide in the degradation of Orange G dye over other oxides is that they are nonpoisonous, insoluble in water, highly surface area and reusability performance [24].

The photocatalytic degradation of Orange G dye over other zirconium oxide samples (Z1, Z2, Z4, Z5, Z6 and Z7) at the optimum conditions (UV + Catalyst + H<sub>2</sub>O<sub>2</sub> for 180 min) was in the following order; Z5 (97.20%) > Z2 (96.17%) > Z1 (95.98%) > Z4 (95.47%) > Z7 (95.26%) > Z6 (94.89%).

#### 4. Conclusion

Different inexpensive organic acids were used as precursors for the preparation of zirconium oxide nanoparticles (Z1–Z7) via precipitation – ignition route with average crystal size and optical energy gap of (9.9 nm, 4.30 eV), (8.3 nm, 1.80 eV), (7.1 nm, 2.70 eV), (11.3 nm, 3.00 eV), (7.3 nm, 2.70 eV), (35.6 nm, 2.80 eV) and (26.0 nm, 2.90 eV) using oxalic, tartaric, citric, succinic, malic, maleic and malonic acids, respectively. All the prepared oxides give the main peaks of FT-IR bands around 498, 3444 and 1633 cm<sup>-1</sup> which are assigned to Zr–O stretching, OH stretching and H–O–H bending vibrations, respectively. The UV photocatalytic degradation of Orange G dye over the as-prepared zirconium oxide (Z3), in presence of hydrogen peroxide, showed the highest percent of degradation (100%) within 180 min.

#### Acknowledgments

The authors gratefully acknowledge Dr. Ehab A. Abdelrahman (Chemistry department, Faculty of Science, Benha University) for his great effort and high experience in helping us in the preparation of nanomaterials and its application in dye removal and also for helping us in the interpretation of the results.

#### References

- B. Neppolian, Q. Wang, H. Yamashita, H. Choi, Synthesis and characterization of ZrO<sub>2</sub>-TiO<sub>2</sub> binary oxide semiconductor nanoparticles: application and interparticle electron transfer process, *Appl. Catal. A Gen.* 15 (2007) 264–271.
- Z. Zhao, J. Ran, Sulphated mesoporous La<sub>2</sub>O<sub>3</sub>-ZrO<sub>2</sub> composite oxide as an efficient and reusable solid acid catalyst for alkenylation of aromatics with phenylacetylene, *Appl. Catal. A Gen.* 503 (2015) 77–83.
- K.C. Soni, S.C. Shekar, B. Singh, T. Gopi, Catalytic activity of Fe/ZrO<sub>2</sub> nanoparticles for dimethyl sulfide oxidation, *J. Colloid Interface Sci.* 446 (2015) 226–236.
- H.A. Lara-García, I.C. Romero-Ibarra, H. Pfeiffer, Hierarchical Na-doped cubic ZrO<sub>2</sub> synthesis by a simple hydrothermal route and its application in biodiesel production, *J. Solid State Chem.* 218 (2014) 213–220.
- A. Słowska, J. Kaszewski, E. Wolska-Kornio, B. Witkowski, Ł. Wachnicki, E. Mijowska, V. Karakitsou, Z. Gajewski, M. Godlewski, M.M. Godlewski, Luminescent properties of ZrO<sub>2</sub>: Tb nanoparticles for applications in neuroscience, *Opt. Mater.* (2016) (in press).
- I. Atkinson, I. Teoreanu, O.C. Mocioiu, M.E. Smith, M. Zaharescu, Structure property relations in multicomponent oxide systems with additions of TiO<sub>2</sub> and ZrO<sub>2</sub> for glaze applications, *J. Non-Cryst. Solids* 356 (2010) 2437–2443.
- S. Li, Y. Jiao, Z. Wang, W. Jianli, Z. Quan, L. Xiangyuan, C. Yaoqiang, Performance of RP-3 kerosene cracking over Pt/WO<sub>3</sub>-ZrO<sub>2</sub> catalyst, *J. Anal. Appl. Pyrolysis* 113 (2015) 736–742.
- A. Fakhri, S. Behrouz, I. Tyagi, S. Agarwal, V.K. Gupta, Synthesis and characterization of ZrO<sub>2</sub> and carbon-doped ZrO<sub>2</sub> nanoparticles for photocatalytic application, *J. Mol. Liq.* 216 (2016) 342–346.
- E.D. Sherly, J.J. Vijaya, N.C.S. Selvam, L.J. Kennedy, Microwave assisted combustion synthesis of coupled ZnO-ZrO<sub>2</sub> nanoparticles and their role in the photocatalytic degradation of 2,4-dichlorophenol, *Ceram. Int.* 40 (2014) 5681–5691.
- X. Qu, D. Xie, L. Cao, F. Du, Synthesis and characterization of TiO<sub>2</sub>/ZrO<sub>2</sub> coaxial core-shell composite nanotubes for photocatalytic applications, *Ceram. Int.* 40 (2014) 12647–12653.
- P. Bansal, G.R. Chaudhary, S.K. Mehta, Comparative study of catalytic activity of ZrO<sub>2</sub> nanoparticles for sonocatalytic and photocatalytic degradation of cationic and anionic dyes, *Chem. Eng. J.* 280 (2015) 475–485.
- T. Sreethawong, S. Ngamsinlapasathian, S. Yoshikawa, Synthesis of crystalline mesoporous-assembled ZrO<sub>2</sub> nanoparticles via a facile surfactant-aided sol-gel process and their photocatalytic dye degradation activity, *Chem. Eng. J.* 228 (2013) 256–262.
- L. Renuka, K.S. Anantharaju, S.C. Sharma, H.P. Nagaswarupa, S.C. Prashantha, H. Nagabhushana, Y.S. Vidya, Hollow microspheres Mg-doped ZrO<sub>2</sub> nanoparticles: green assisted synthesis and applications in photocatalysis and photoluminescence, *J. Alloys Compd.* 672 (2016) 609–622.
- A.A. Ashkarran, S.A.A. Afshar, S.M. Aghigh, K. Mona, Photocatalytic activity of ZrO<sub>2</sub> nanoparticles prepared by electrical arc discharge method in water, *Polyhedron* 29 (2010) 1370–1374.
- K. Anandan, V. Rajendran, A low-temperature synthesis and characterization of tetragonal-ZrO<sub>2</sub> nanoparticles via simple hydrothermal process, *J. Phys. Sci.* 17 (2013) 179–184.
- M.R.H. Siddiqui, A.I. Al-Wassil, A.M. Al-Otaibi, R.M. Mahfouz, Effects of precursor on the morphology and size of ZrO<sub>2</sub> nanoparticles, synthesized by sol-gel method in non-aqueous medium, *Mater. Res.* 15 (6) (2012) 986–989.
- A.I.Y. Tok, F.Y.C. Boey, S.W. Du, B.K. Wong, Flame spray synthesis of ZrO<sub>2</sub> nanoparticles using liquid precursors, *Mater. Sci. Eng. B* 130 (2006) 114–119.
- H. Kil, S. Wang, J. Ryu, D. Lim, S. Cho, Glycothermal synthesis of nanocrystalline ZrO<sub>2</sub> powders at low temperature without mineralizers, *J. Ceram. Soc. Jpn.* 120 (2012) 52–57.
- A. Bahari, M. Ghanbari, Low temperature synthesis of ZrO<sub>2</sub> and CrO<sub>2</sub> by sol-gel process, *Int. J. Chem. Tech. Res.* 3 (2011) 1686–1691.
- A. Chen, Y. Zhou, S. Miao, Y. Li, W. Shen, Assembly of monoclinic ZrO<sub>2</sub> nanorods: formation mechanism and crystal phase control, *Cryst. Eng. Comm.* 18 (2016) 580–587.
- H. R. Sahu, G. Rao Ranga, Characterization of combustion synthesized zirconia powder by UV-vis, IR and other techniques, *Bull. Mater. Sci.* 23 (2000) 349–354.
- S.L. Dhare, Silica-zirconia alkali-resistant coatings by sol-gel route, *Curr. Sci.* 108 (2015) 1647–1652.
- S. Zinatloo-Ajabshir, M. Salavati-Niasari, Facile route to synthesize zirconium dioxide (ZrO<sub>2</sub>) nanostructures: structural, optical and photocatalytic studies, *J. Mol. Liq.* 216 (2016) 545–551.
- H.M. Aly, M.E. Moustafa, M.Y. Nassar, E.A. Abdelrahman, Synthesis and characterization of novel Cu (II) complexes with 3-substituted-4-amino-5-mercapto-1,2,4-triazole Schiff bases: a new route to CuO nanoparticles, *J. Mol. Struct.* 1086 (2015) 223–231.